Shape transition and migration of $TiSi_2$ nanostructures embedded in a Si matrix

Cite as: J. Appl. Phys. **110**, 094304 (2011); https://doi.org/10.1063/1.3657947
Submitted: 11 May 2011 • Accepted: 28 September 2011 • Published Online: 02 November 2011

Anderson Sunda-Meya, David J. Smith and Robert J. Nemanich

Shape transition and migration of $TiSi_2$ nanostructures embedded in a Si matrix

Anderson Sunda-Meya,[1,a)] David J. Smith,[2] and Robert J. Nemanich[2]
[1]*Department of Physics, Xavier University of Louisiana, New Orleans, Louisiana 70125, USA*
[2]*Department of Physics, Arizona State University, Tempe, Arizona 85287, USA*

(Received 11 May 2011; accepted 28 September 2011; published online 2 November 2011)

This study establishes that under conditions of epitaxial Si deposition, embedded Ti-silicide nanostructures undergo shape transitions and migrate upward to the surface during capping with a thin epitaxial Si layer. Many of these structures display a near-hemispherical shape which is attributed to minimization of their surface and interface energies. The density and size of the nanostructures are observed to be temperature-dependent. The buried islands induce inhomogeneous stress profiles on the capping layer surface. Atomic-force micrographs of the islands show square holes at the surface aligned along [110] directions which suggests that the sloping surfaces of the pits approximate to (111) surfaces, and the silicide interface is also facetted to match Si (111) planes. Cross-sectional electron micrographs reveal that many islands display faceting. The observed structural changes can be rationalized in terms of the interplay between thermodynamics and kinetics, solid-state capillarity, and the roughening transition. © *2011 American Institute of Physics*. [doi:10.1063/1.3657947]

I. INTRODUCTION

Titanium silicide has become widely integrated into microelectronic devices as a contact material due to its low electrical resistivity, metallurgical stability, and electrical isolation from the substrate via the Schottky barrier.[1–7] Silicide island structures have attracted much recent attention since they spontaneously form into epitaxial dots or nanowires,[8–17] which are likely to find applications as low-resistance interconnects or as nanoelectrodes for molecular attachment. Understanding the formation and evolution of these nanostructures may lead to approaches for controlling the fabrication of novel nanoscale devices as well as providing better knowledge of fundamental surface phenomena such as thin film growth, strain, surface diffusion, and island ripening.

The properties of these nanostructures are a sensitive function of their size and shape. Therefore, information about their evolution with temperature and time as well as their energetic state relative to thermodynamic equilibrium are significant. Indeed, single electron tunneling characteristics have been observed in $TiSi_2$ nanoislands even at room temperature.[8,18] In another study, distinctive island migration and coalescence was observed for $TiSi_2$ epitaxial islands on Si surfaces.[19] It was found that the coalescence of islands was not caused by random island motion but was instead due to island migration directed toward other islands. This migration mechanism significantly affected evolution of the island distribution.

In this study, we report on the evolution of $TiSi_2$ nanostructures embedded in a Si matrix. We establish that these nanostructures undergo shape transitions and "migrate" to the surface under conditions suitable for epitaxial Si deposition.

II. EXPERIMENTAL

The samples were grown by molecular beam epitaxy (MBE) on Si (001) $\pm 0.5^\circ$ substrates (n- or *p*-type, B- or P-doped, 25-mm-diameter, 20-mm-thick, 0.8 to 1.2 $\Omega \cdot$ cm resistivity with one side polished). The wafers were cleaned by UV-ozone exposure and then treated with an HF-spin etch ($HF:H_2O$:Ethanol = 1:1:10). After chemical cleaning, the wafers were loaded into the ultrahigh-vacuum MBE chamber (base pressure $<2 \times 10^{-10}$ Torr), and heat-cleaned at 900 °C. After *in situ* annealing, low-energy electron diffraction (LEED) patterns of the Si(100) wafer exhibited sharp, double-domain 2×1 surface reconstruction, and Auger electron spectroscopy indicated carbon or oxygen at the noise level of the system.

A Thermionics HM^2 electron-beam evaporator powered by a 10 kW Temescal Simba2 power supply was used to deposit silicon. The e-beam was controlled by a Temescal electron-beam sweep controller and the evaporator was water-cooled to dissipate excess energy and to prevent the evaporator crucibles from melting. An Inficon quartz crystal sensor was used to monitor and control the evaporation rates. The wafer was heated through a coiled, toroidal-shaped and resistively heated tungsten filament. A thermocouple in the middle of the toroidal heater loop measured the temperature of the backside of the wafer.

The deposition of thin Ti films was achieved by the sublimation of titanium from resistively heated Ti filaments. The deposition rate was controlled by the current through the filament and ranged from 0.01 to 0.2 nm/s. The thickness of the deposited Ti was also measured by the Inficon quartz crystal monitor. The average deposition rate was 0.15 nm/s at 750 °C. During Ti deposition, the pressure increased to about 4×10^{-9} Torr.

In the first stage of these experiments, Si(001) substrates with a Si buffer layer of 20 nm were seeded with an array of

a)Electronic mail: asundame@xula.edu.

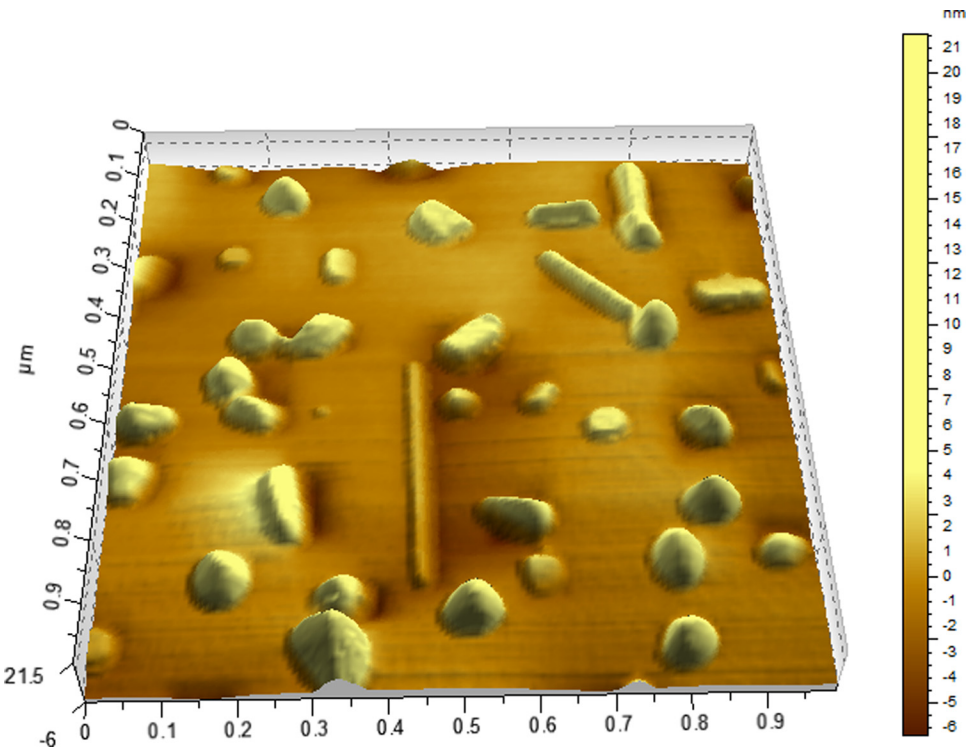

FIG. 1. (Color online) AFM micrograph showing $TiSi_2$ islands grown spontaneously by depositing 0.5 nm Ti at 750 °C onto Si(100) with a 20-nm Si buffer layer. Different types of islands are formed.

coherent, multifaceted nanostructures, namely wires and islands, by depositing ~0.5 nm of titanium at 750 °C and annealing for 2 min. The island-covered surfaces were then exposed to Si flux. Two different sets of samples were grown. In one sample set, a 20-nm-thick Si capping layer was deposited with the substrate temperature held at 550, 650, 750, 850, 950, and 1050 °C. In the second set of samples, capping layers of thickness 20, 40, 60, 80, and 100 nm were deposited at constant substrate temperatures of 550, 750, and 1050 °C.

The surface morphology was studied in contact mode with an Autoprobe CP-R atomic force microscope (AFM) at room temperature and ambient atmosphere, utilizing an Si cantilever with a spring constant of 1.6N/m and a resonant frequency of 170 kHz. An Asylum Research AFM MFP-3D with a standard optical lever was also used. Further observations were made with a JEOL 4000EX high-resolution transmission electron microscope (TEM) operated at 400 keV. Cross-section samples were prepared for examination in [110]-type zone-axis projections using standard methods of mechanical polishing, dimpling, ion-beam milling to perforation. Diffraction contrast images were recorded with a small objective aperture to highlight defect microstructure, while high-resolution images were recorded at optimum defocus so that the positions of atomic columns appeared with dark contrast. All TEM micrographs shown in the text have the Si(001) substrate normal vertically upwards.

III. RESULTS

Titanium disilicide islands and nanowires (NWs) form spontaneously on Si(001) by reactive deposition as shown by the typical AFM micrograph in Fig. 1. Different island types are observed, having different orientations relative to the substrate.[12,20,21] Fig. 2 shows several cross-sectional electron micrographs, recorded with the Si(110) zone-axis parallel to the electron-beam direction, indicating that islands can have either flat tops or long flat interfaces, parallel to the Si(001) surface plane (a) and (c), while others display faceted cross-sections with a tendency toward alignment with the Si(111) planes. Wires often have a triangular shape corresponding to end-on projections as seen previously.[15] All of these

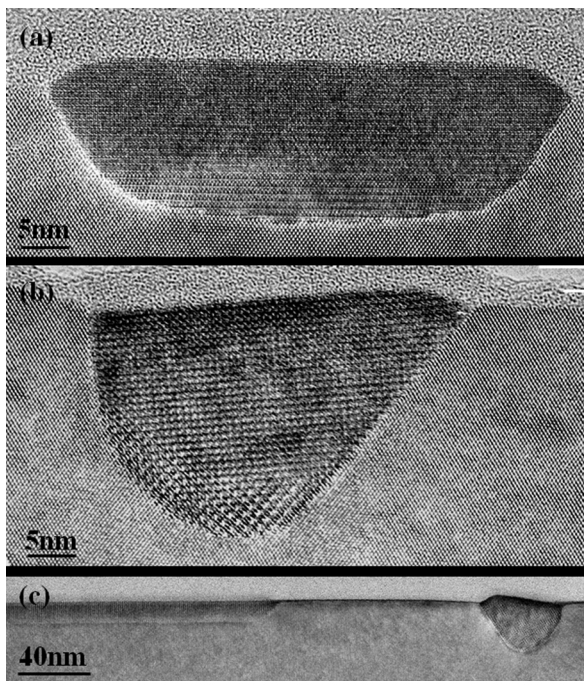

FIG. 2. Cross-section electron micrographs showing different morphologies of $TiSi_2$ islands formed on Si(001). Images recorded along [110]-type zone-axis projection, with substrate normal pointing vertically upward.

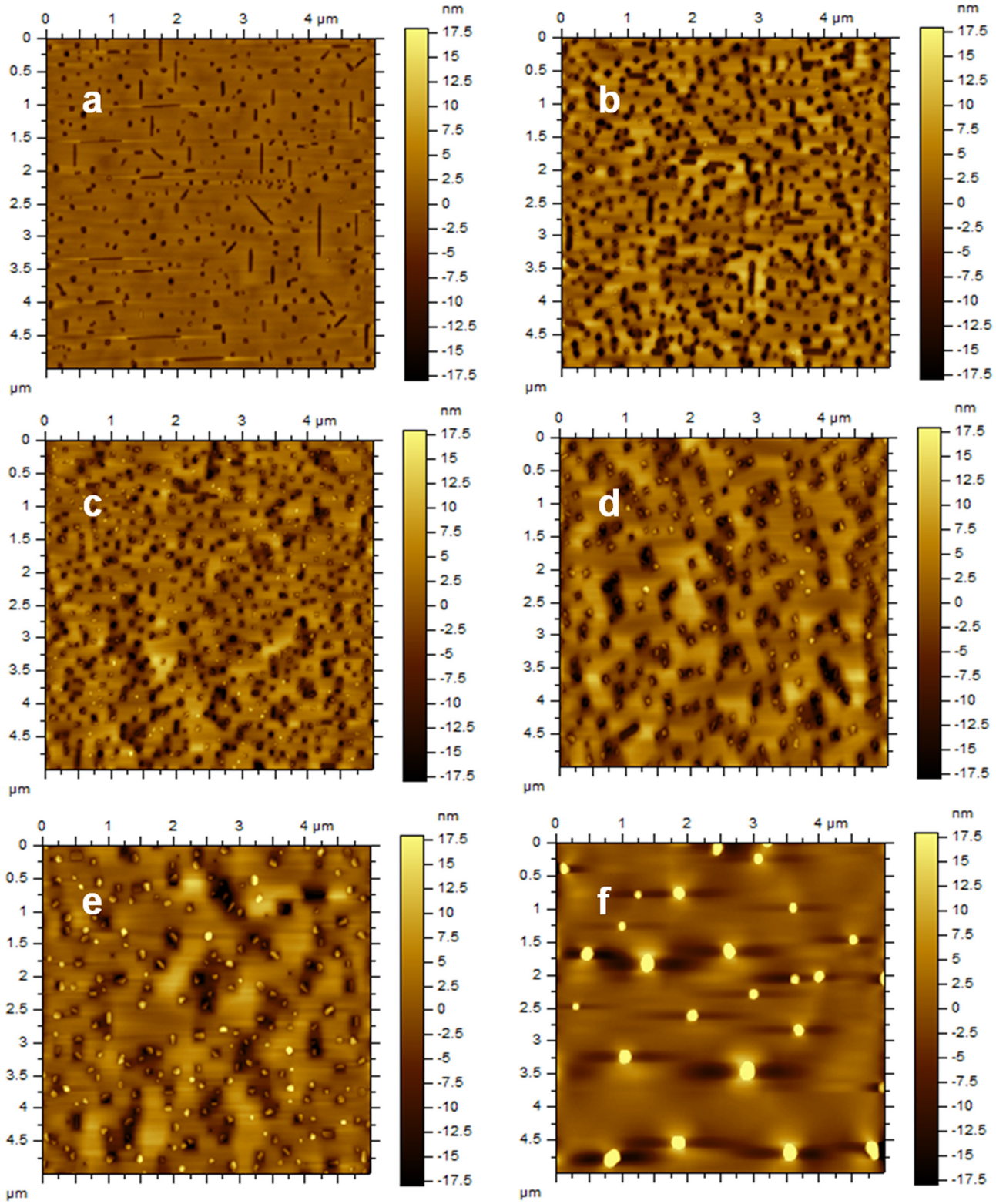

FIG. 3. (Color online) Series of AFM micrographs showing samples grown with 20-nm Si capping layer at temperatures of (a) 550 °C; (b) 650 °C; (c) 750 °C; (d) 850 °C; (e) 950 °C; and (f) 1050 °C.

nanostructures present on the Si surface are recessed into the silicon substrate due to the endotaxial growth mechanism.[16]

Figure 3 shows a series of AFM micrographs of the samples with 20-nm-thick capping layers, grown at temperatures ranging from 550 to 1050 °C. For the 550 °C capping layer, very shallow pits are evident suggesting that the Si layer partially covers most wires and islands which appear to be buried beneath the surface. For deposition at 650 °C and above, the surfaces are dominated by deeper pits which appear to correspond to the islands and wires. Some wires appear to be

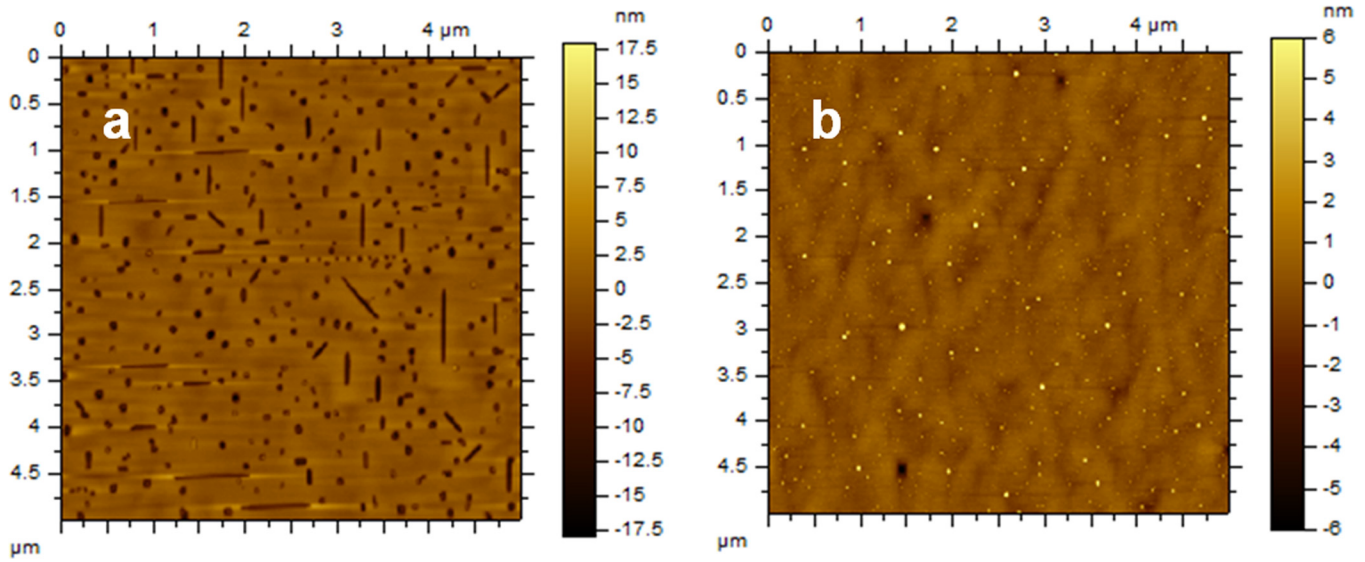

FIG. 4. (Color online) AFM images of two samples with Si deposition at 550 °C and Si thickness of (a) 20 nm and (b) 100 nm.

breaking into sections or islands. The density of island-shaped pits decreases with increasing temperatures to 950 °C while the island size increases.

Figure 4 shows that deposition of 100 nm of Si at 550 °C results in a smooth surface with evidently buried nanostructures, although a few square holes are still visible, aligned along the equivalent ⟨110⟩ directions. [The small particles on the surface are attributed to surface contamination from ambient exposure. We suspect that some of the small particles evident in Fig. 3(c) and 3(d) are also due to contamination from ambient exposure, which depends on the local air quality and the ambient exposure time prior to the AFM measurements.]

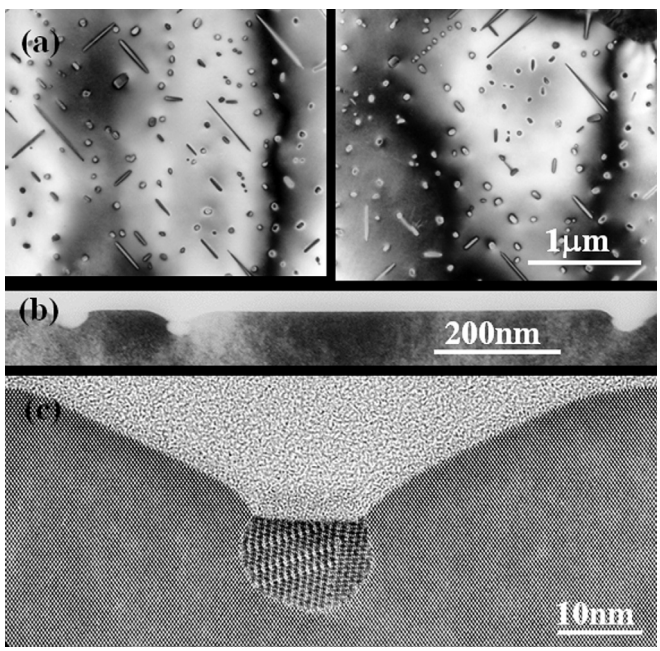

FIG. 5. (a) Plane-view electron micrograph of $TiSi_2$ nanostructures covered by 20-nm Si deposited at 550 °C. Needle-like nanowires are visible aligned along the equivalent orthogonal ⟨110⟩ directions (the long-range darker contrast is attributable to local crystal bending); (b) and (c) Cross-section electron micrographs showing hemispherical and droplet-shaped islands.

The plane-view TEM image of the 20 nm, 550 °C sample in Fig. 5(a) shows islands and wire-like islands aligned in two orthogonal directions, while cross-sectional images show droplet-like islands either at the surface [Fig. 5(b)] or recessed into the surface [Fig. 5(c)]. The top surface plane of the latter structure is flat and oriented along the ⟨001⟩ direction and may correspond to the planes of the square holes visible in the AFM scans.

The change in surface morphology with increasing Si capping-layer thickness at 750 °C is shown in Fig. 6. After deposition of a 20 nm Si capping layer, the AFM image displays a high density of pits which correspond to the $TiSi_2$ islands. Small pits correspond to individual separated islands while larger pits apparently indicate nearby or coalesced islands. The density of small pits decreases as the capping layer thickness is increased, but the density of larger pits appears to remain constant. Cross-section electron micrographs of the 20 nm capping layer sample shown in Fig. 7 reveal droplets or hemispherical islands near the surface. Some islands below the surface exhibit sides with flat interfaces in the ⟨001⟩ direction. The trend seems to be that smaller faceted islands are covered with the capping layer while larger islands tend to form hemispherical shapes and maintain exposure to the surface at the bottom of a pit. The trend continues as the Si capping-layer thickness is increased, as shown by the cross-section electron micrograph in Fig. 8. Hemispherical islands with flat tops are observed at the bottom of pits, as well as rounded elliptical islands that extend well below the surface. Several buried small islands are also evident, with some of them showing only very weak contrast.

When the substrate temperature during Si deposition is increased to 1050 °C, the buried nanostructures (both wires and islands) appear to become unstable while randomly

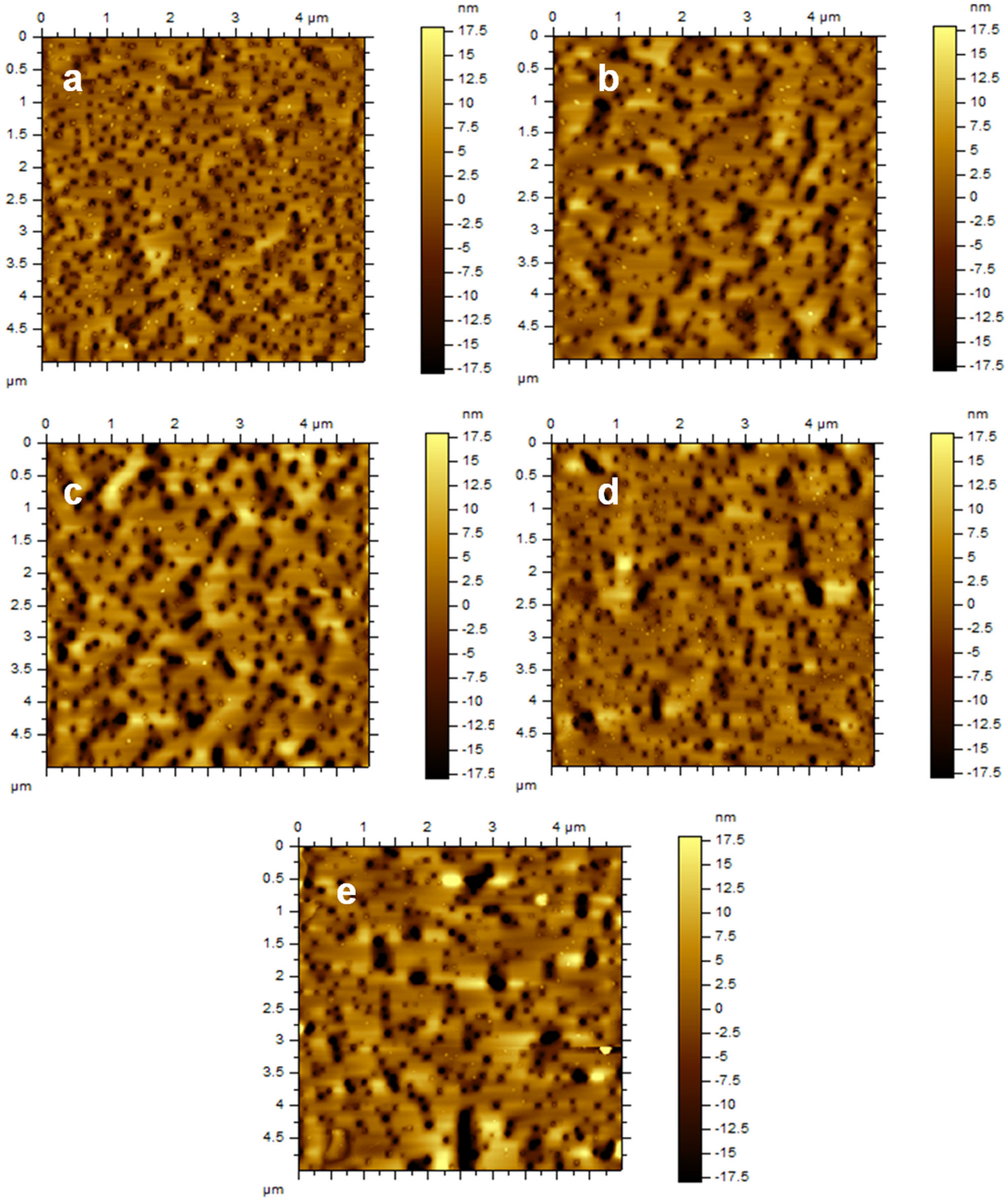

FIG. 6. (Color online) Series of AFM images of samples grown at 750 °C with Si capping layer thicknesses of (a) 20 nm; (b) 40 nm; (c) 60 nm; (d) 80 nm; and (e) 100 nm. Island density decreases with increasing Si thickness, and square holes are evident up to 100 nm.

distributed islands protrude above the surface, as visible in Fig. 9. As the Si deposition thickness is increased, the size of the islands increases and their density decreases, as shown in Fig. 10. It appears that these islands undergo Ostwald ripening on the surface due to the longer annealing period.

From cross-section electron micrographs, two different aligned island structures can be distinguished. The first can be characterized as an island having a long flat interface, parallel to the Si(001) plane, also accompanied by some steps [Fig. 2(a)]; the second type displays a highly faceted cross-section with a tendency toward alignment with the Si (111)

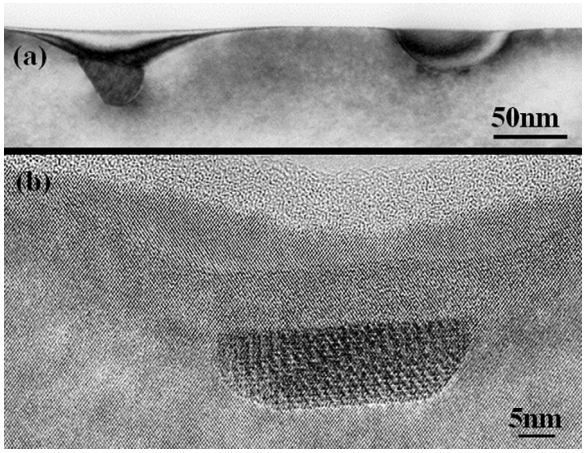

FIG. 7. Cross-section electron micrographs of sample covered by 20 nm Si at 750 °C. Islands exhibit droplet or hemispherical shape, while other islands beneath the surface are faceted, as clearly visible in the island shown enlarged in (b).

planes [Fig. 2(b)]. From selected area electron diffraction patterns in both plane-view and cross section, two different epitaxial relationships can be determined, as previously shown in our group: Si(004)||C49-$TiSi_2$(040) and Si[$2\bar{2}0$]||C49-$TiSi_2$[$00\bar{2}$] for the long flat islands; and Si(002)||C49-$TiSi_2$($00\bar{2}$) and Si[$2\bar{2}0$]||C49-$TiSi_2$[040] for islands with Si(111) steps.[22,23,27] Furthermore, both types have Si[220] ||C49-$TiSi_2$[$\bar{2}$00].

IV. DISCUSSION

$TiSi_2$ islands are formed by nucleation from very thin films and they have larger surface-to-volume ratios than islands formed from thicker films. Thus, they are energetically favored to nucleate in the C49 phase in thin films for temperatures as high as 1200 °C.[24–26] This nucleation behavior in the Ti/Si(100) system has been well described by conventional nucleation theory[25,27,28] over the temperature range 400–1200 °C,[25,29] but recent studies have suggested that the energy due to quantized electronic levels of flat islands could also influence the island morphology.[9]

Ti diffusion is rate-limiting for the relevant range of growth parameters.[30] During Ti deposition at high temperature, Ti adatoms move randomly on the Si surface due to the low solubility of Ti in Si,[13] and they are eventually captured by growing islands. It has been proposed for elongated islands that the Ti atoms attach at the ends as well as at edges. However, Ti adatoms attached at edges will finish up diffusing to the ends since the energy barrier for the nucleation of a new adatom layer is larger at the edges than at the ends.[16,31] The Ti atoms react with Si flux from the substrate or from nearby Si step edges further elongating the islands.[32] Thus, the formation of elongated $TiSi_2$ islands, and their shape transitions, are due to energetics as well as kinetics.

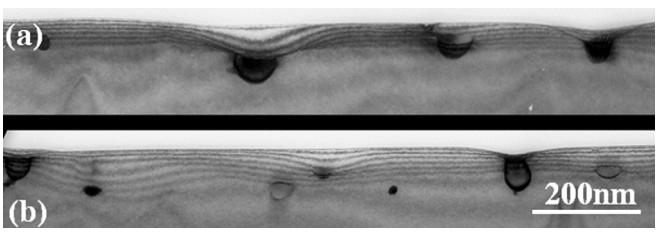

FIG. 8. Cross-section electron micrographs of sample after deposition of 100-nm of Si at 750 °C. Islands appear with darker contrast.

When Si surfaces with $TiSi_2$ islands and wires are capped with Si, three stages that are mostly associated with the Si deposition temperature are observed. At low temperatures (<550 °C), both nanowires and islands are covered and the islands shapes are effectively maintained. At higher temperatures (550 °C < T < 1000 °C), larger islands form which exhibit hemispherical shapes, and they maintain contact with the surface at the base of pits. At the highest temperature studied (1050 °C), islands form above the Si surface and grow in size as the deposition time is increased.

At higher Si deposition temperature (550 °C < T < 1000 °C), the shapes of the islands change to half-spheres touching the surface or to droplet-like islands. Locally, this trend indicates that facetted interface structures are unstable. This appears to correspond to a roughening transition of the $TiSi_2$/Si interface. The roughening transition of a solid surface is attributed to surface diffusion and step stability. In this case we propose that the roughening is enabled by substantial diffusion of Si from the exposed surface, and therefore the Si deposition and diffusion creates a dynamic instability. From the AFM and TEM cross-section images, it can be inferred that these hemispherical shaped islands are terminated in square facetted pits.

At low Si deposition temperature, deposited Si atoms may succeed in covering an island (when more atoms arrive than diffuse through the island), after which homoepitaxy takes place, and the island is buried. Continued exposure at higher temperatures may cause some buried islands to be faceted, as visible in Fig. 7, but islands in contact with the surface maintain a hemispherical or truncated elliptical shape. For the lower temperature depositions (<650 °C), square depressions are evident, which are aligned along the ⟨110⟩ directions of the (001) surface. As indicated in Fig. 5, the islands are often at the bottom of pits, which appear close to (111) surfaces. Similarly, the interfaces of the faceted islands often align with (111) surfaces of the Si substrate. Both of these effects could contribute to the alignment of the islands along ⟨110⟩ directions.

The large islands at 1050 °C appear to be evolving with a type of Ostwald ripening in which larger nanostructures grow at the expense of smaller surrounding structures, as per the Gibbs-Thompson relation:[33]

$$N_r = N_0 \exp(2\gamma\Omega/rkT),$$

where N_r is the adatom concentration for a nucleus of radius r, N_0 is the adatom concentration corresponding to the vapor pressure for the planar surface, γ is the surface energy per unit area, and Ω is the volume per atom. Energy minimization represents the major driving force for island growth. As evidenced in Fig. 10, the average island size increases while their density decreases with continued deposition and

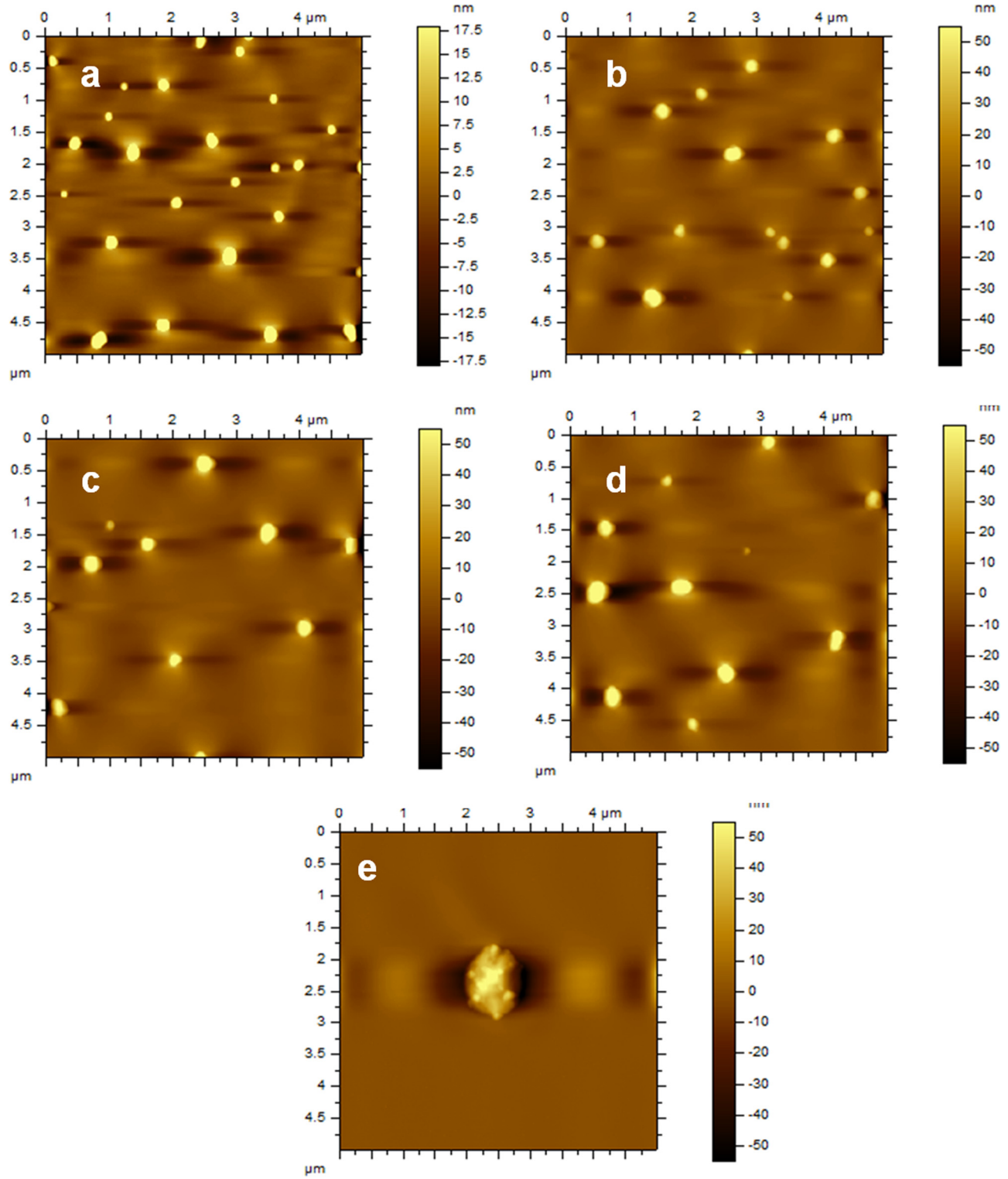

FIG. 9. (Color online) Series of AFM images for samples with Si deposited at constant substrate temperature of 1050 °C and thicknesses of (a) 20 nm; (b) 40 nm; (c) 60 nm; (d) 80 nm; and (e) 100 nm, as shown.

annealing at 1050 °C. These islands have also made a transition to surface islands instead of buried epitaxial islands, and this effect may be driven by the larger surface energy of the C54 phase compared to C49.[25]

The square holes at the surface are aligned along the ⟨110⟩ directions, as shown by previous studies in our group.[22] The epitaxial relationships for the two types of islands shown in Fig. 2 provide two directions parallel to the Si⟨110⟩ directions. A closely matching interplanar spacing normal to either side of the interface is believed to represent a favorable condition for epitaxy,[34] because some kind of superstructure often exists in such cases. There is a good match between the Si(110)-planes ($d_{Si(110)} = 3.84$ Å) and the C49-$TiSi_2$(100) and (001) planes ($d_{C49(100)} = 3.62$ Å) (5.7% mismatch) and $d_{C49(001)} = 3.60$ Å (6.3% mismatch).[22,26]

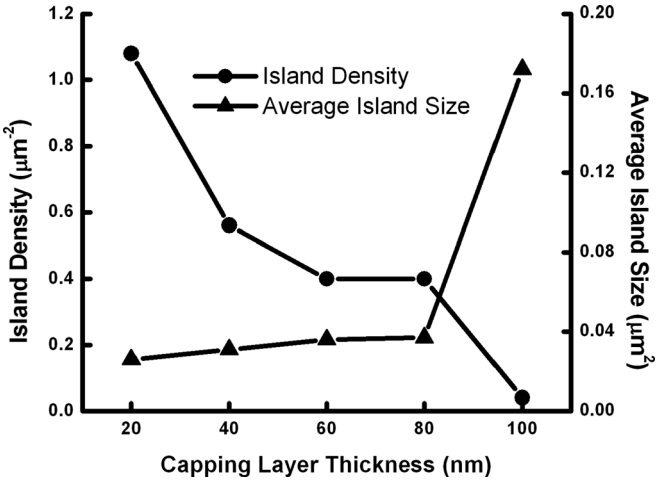

FIG. 10. Plot showing variation in average island size and island density as a function of capping layer thickness, for temperature maintained at 1050 °C during Si deposition.

V. CONCLUSIONS

$TiSi_2$ islands grown on Si(001) substrates were capped by Si epilayers at temperatures ranging from 550 to 1050 °C. The capping layer thicknesses ranged from 20 to 100 nm. The wires were unstable at high temperature and coverage. Most islands extended below the surface and underwent a transition where facetted surfaces became unstable. An increase in the Si deposition temperature and thickness generally resulted in square pits at the surface aligned along the ⟨110⟩ directions. The buried silicide islands then changed from droplet to elliptical shapes or became half-spherical touching the surface. At high temperatures, the islands migrated to the surface and were coarsened. We proposed that the island shape transition is related to Si diffusion through the particle and indicates a complicated interplay of kinetics and energetics.

ACKNOWLEDGMENTS

This work was supported by National Science Foundation Grant No. DMR-0512591. We acknowledge Yang Sun for her assistance in refining the AFM scans. The experimental measurements were completed while AS-M and RJN were at North Carolina State University. We also acknowledge use of facilities in the John M. Cowley Center for High Resolution Electron Microscopy at Arizona State University.

[1]T. Aoki, K. Shudo, K. Sato, S. Ohno, H. Nishioka, T. Lida, M. Toramaru, and M. Tanaka, Appl. Surf. Sci. **256**, 1191 (2009).
[2]L. F. Hao and P. A. Bennett, Nanotechnology **20**, 355201 (2009).
[3]T. Soubiron, R. Stiufiuc, L. Patout, D. Deresmes, B. Grandidier, D. Stievenard, J. Koble, and M. Maier, Appl. Phys. Lett. **90**, 102112 (2007).
[4]P. A. Bennett and H. v. Kaenel, J. Phys. D **32**, R71 (1999).
[5]R. T. Tung, Appl. Surf. Sci. **117–118**, 268 (1997).
[6]A. H. Reader, A. H. van Ommen, P. J. W. Weijs, R. A. M. Wolters, and D. J. Oostra, Rep. Prog. Phys. **56**, 1397 (1993).
[7]B. Mohadjeri, K. Maex, R. A. Donaton, and H. Bender, J. Electrochem. Soc. **146**, 1122 (1999).
[8]J. L. Tedesco, J. E. Rowe, and R. J. Nemanich, J. Appl. Phys. **107**, 123715 (2010).
[9]S. Manor, J. K. Tripathi, and I. Goldfarb, J. Mater. Sci. **45**, 6313 (2010).
[10]M. Toramaru, T. Iida, K. Sato, S. Ohno, K. Shudo, Y. Morikawa, and M. Tanaka, J. Phys. Condens. Matter **20**, 485006 (2008).
[11]A. W. Stephenson and M. E. Welland, J. Appl. Phys. **78**, 5143 (1995).
[12]G. Medeiros-Ribeiro, D. A. A. Ohlberg, D. R. Bowler, R. E. Tanner, G. A. D. Briggs, and R. S. Williams, Surf. Sci. **431**, 116 (1999).
[13]G. A. D. Briggs, D. P. Basile, G. Medeiros-Ribeiro, T. I. Kamins, D. A. A. Ohlberg, and R. S. Williams, Surf. Sci. **457**, 147 (2000).
[14]I. Goldfarb and G. A. D. Briggs, Phys. Rev. B **60**, 4800 (1999).
[15]M. Stevens, Z. He, D. J. Smith, and P. A. Bennett, J. Appl. Phys. **93**, 5670 (2003).
[16]Z. He, D. J. Smith, and P. A. Bennett, Phys. Rev. Lett. **93**, 256102 (2004).
[17]Y. C. Chou, K. C. Lu, and K. N. Tu, Mater. Sci. Eng. R. **70**, 112 (2010).
[18]J. Oh, V. Meunier, H. Ham, and R. J. Nemanich, J. Appl. Phys. **92**, 3332 (2002).
[19]W.-C. Yang, M. Zeman, H. Ade, and R. J. Nemanich, Phys. Rev. Lett. **90**, 136102 (2003).
[20]K. Saito, Y. Higashi, T. Amazawa, and Y. Arita, J. Electrochem. Soc. **141**, 1879 (1994).
[21]K. Saito and Y. Arita, J. Electrochem. Soc. **143**, 3778 (1996).
[22]B. L. Kropman, C. A. Sukow, and R. J. Nemanich, Mater. Res. Soc. Symp. Proc. **280**, 589 (1993).
[23]C. A. Sukow and R. J. Nemanich, J. Mater. Res. **9**, 1214 (1994).
[24]W. Yang, F. J. Jedema, H. Ade, and R. J. Nemanich, Thin Solid Films **308–309**, 627 (1997).
[25]H. Jeon, C. A. Sukow, J. W. Honeycutt, G. A. Rozgonyi, and R. J. Nemanich, J. Appl. Phys. **71**, 4269 (1992).
[26]Z. He, M. Stevens, D. J. Smith, and P. A. Bennett, Surf. Sci. **524**, 148 (2003).
[27]J. A. Venables, Surf. Sci. **299/300**, 798 (1994).
[28]H. Brune, Surf. Sci. Rep. **31**, 121 (1998).
[29]K. Ishiyama, Y. Taga, and A. Ichimiya, Surf. Sci. **349**, 267 (1996).
[30]T. H. McDaniels, J. A. Venables, and P. A. Bennett, Phys. Rev. Lett. **87**, 17605 (2001).
[31]M. Kastner and B. Voigtlander, Phys. Rev. Lett. **82**, 2745 (1999).
[32]R. M. Tromp, Phys. Rev. Lett. **81**, 1050 (1998).
[33]K. N. Tu, J. W. Mayer, and L. C. Feldman, *Electronic Thin Film Science: for Electrical Engineers and Materials Scientists* (Macmillan, New York, 1992).
[34]A. Catana, P. E. Schmid, M. Heintze, F. Lévy, P. Stadelmann, and R. Bonnet, J. Appl. Phys. **67**, 1820 (1990).